

# Mismatched Models to Lower Bound the Capacity of Dual-Polarization Optical Fiber Channels

Francisco Javier García-Gómez and Gerhard Kramer, *Fellow, IEEE*

**Abstract**—Regular perturbation is applied to the Manakov equation and motivates a generalized correlated phase-and-additive noise model for wavelength-division multiplexing over dual-polarization optical fiber channels. The model includes three hidden Gauss-Markov processes: phase noise, polarization rotation, and additive noise. Particle filtering is used to compute lower bounds on the capacity of multi-carrier communication with frequency-dependent powers and delays. A gain of 0.17 bits/s/Hz/pol in spectral efficiency or 0.8 dB in power efficiency is achieved with respect to existing models at their peak data rate. Frequency-dependent delays also increase the spectral efficiency of single-polarization channels.

**Index Terms**—Achievable rate, dual-polarization, optical fiber, phase noise, regular perturbation.

## I. INTRODUCTION

Dual-polarization (2-pol) transmission almost doubles the data rates of optical fiber links [1], [2]. The apparent small reduction from a factor of two is caused by nonlinear coupling of polarizations due to the Kerr effect [3], [4]. A spectral efficiency upper bound of  $\log_2(1 + \text{SNR})$  bits/s/Hz/pol follows by generalizing [5], [6] to the 2-pol Manakov equation, where SNR is the receiver signal-to-noise ratio.

Simplified versions of the nonlinear Schrödinger equation (NLSE) can serve as mismatched models to compute capacity lower bounds for 1-pol channels, see the review in [7]. For example, capacity bounds for 1-pol channels are derived in [8] by using wavelength-division multiplexing (WDM) and a conditionally Gaussian model where the noise variance depends on the amplitude of the transmitted symbol. The Gaussian Noise [9] and Enhanced Gaussian Noise [10] models refine this approach, also for 2-pol channels, by giving analytical expressions for the power spectral density (PSD) of the nonlinear interference that is assumed to be Gaussian.

The regular perturbation (RP) model [11]–[14] of the NLSE leads to correlated phase noise models [15]–[17] and improved capacity bounds for 1-pol. There is less literature on RP for 2-pol: we have found analyses only for special input signals such as Gaussian pulses [18] or Fourier series with random Gaussian coefficients [19]. A logarithmic perturbation (LP) model is developed in [20], [21] that suggests a time- and frequency-varying polarization and phase noise (PPN) model. The latter model, together with WDM and multiple carriers per wavelength, was used in [4] to compute the best 2-pol capacity bounds that we are aware of.

Date of current version April 19, 2021. This work was supported by the German Research Foundation (DFG) under Grants KR 3517/8-1 and 3517/8-2. (Corresponding author: Francisco Javier García-Gómez.)

The authors are with the Institute for Communications Engineering, Technical University of Munich, 80333 Munich, Germany (e-mail: javier.garcia@tum.de; gerhard.kramer@tum.de).

We used RP in [22] to develop a correlated phase-and-additive noise (CPAN) model for WDM for 1-pol transmission. The model improved the capacity bounds in [23] by applying a whitening filter and multi-carrier communication with frequency-dependent power allocation (FDPA). We here extend the CPAN model to 2-pol. The proposed 2pCPAN model includes phase noise, a random polarization rotation, and additive noise. All three impairments are correlated in time and the phase noise is correlated across polarizations. Using multiple carriers per wavelength, FDPA, and frequency-dependent delays, 2pCPAN improves the rates in [4] by 0.17 bits/s/Hz/pol in spectral efficiency or 0.8 dB in power efficiency at the peak data rate.

This paper is organized as follows. Sec. II describes notation and the 2-pol propagation model. Sec. III develops continuous- and discrete-time RP models. Sec. IV presents the 2pCPAN model and Sec. V simplifies the model to make it suitable for computing information rates. Sec. VI explains how to compute lower bounds on capacity. Sec. VII describes the multi-carrier approach with FDPA and Sec. VIII provides numerical capacity lower bounds. Sec. IX concludes the paper.

## II. PRELIMINARIES

### A. Notation

We use similar notation as in [22]. For instance, the Fourier transform of a function  $u(t)$  is

$$\mathcal{F}(u(t)) = \mathcal{F}(u(t))(\Omega) = \int_{-\infty}^{\infty} u(t)e^{-j\Omega t} dt \quad (1)$$

and the inverse Fourier transform of  $U(\Omega)$  is  $\mathcal{F}^{-1}(U(\Omega)) = \mathcal{F}^{-1}(U(\Omega))(t)$ . The dispersion operator  $\mathcal{D}_z$  is defined as

$$\mathcal{D}_z u(t) = \mathcal{F}^{-1}\left(e^{j\frac{\beta_2}{2}\Omega^2 z} \mathcal{F}(u(t))\right) \quad (2)$$

which is the same as a convolution with an all-pass filter with the spectrum  $e^{j\frac{\beta_2}{2}\Omega^2 z}$ .

Fourier transforms, dispersion operators, and convolutions are linear operators  $L$  for which we write

$$Lu(t) = \int_{-\infty}^{\infty} u(\tau)K(\tau, t) d\tau \quad (3)$$

$$L^*v(t) = \int_{-\infty}^{\infty} v(\tau)K(t, \tau)^* d\tau \quad (4)$$

where  $K$  is the kernel function and  $L^*$  is the adjoint of  $L$ . We have the inner-product property

$$\int_{-\infty}^{\infty} Lu(t)v(t)^* dt = \int_{-\infty}^{\infty} u(t)(L^*v(t))^* dt. \quad (5)$$

A two-polarization signal is written as a vector  $\mathbf{u} = (u, \bar{u})^T$ . For vectors, the operators  $\mathcal{F}$ ,  $\mathcal{F}^{-1}$  and  $\mathcal{D}_z$  are applied entry-wise to the components. We consider unit-energy sinc-pulses

$$s(t) = \frac{1}{\sqrt{T}} \text{sinc}\left(\frac{t}{T}\right) \quad (6)$$

where  $\text{sinc}(x) := \sin(\pi x)/(\pi x)$  and  $T$  is the symbol period.

### B. Dual-Polarization Propagation Model

Consider an optical fiber of length  $\mathcal{L}$ . The polarization state of a signal changes randomly along the fiber due to randomly varying birefringence. If the change is fast enough, then the propagation of a 2-pol signal  $\mathbf{u}(z, t)$  is described by the Manakov equation [24], [25]:

$$\frac{\partial}{\partial z} \mathbf{u} = -j \frac{\beta_2}{2} \frac{\partial^2}{\partial t^2} \mathbf{u} + j \gamma f(z) \|\mathbf{u}\|^2 \mathbf{u} + \frac{1}{\sqrt{f(z)}} \mathbf{n} \quad (7)$$

where  $z$  is distance,  $t$  is time,  $\beta_2$  is the dispersion coefficient, and  $\gamma = (8/9)2\pi n_2/(\lambda A_{\text{eff}})$  is the nonlinear coefficient.  $A_{\text{eff}}$  is the effective area of the fiber,  $n_2$  is the nonlinear index coefficient,  $\lambda$  is the transmission wavelength, and the factor  $8/9$  is due to the randomly varying birefringence. The scalar function  $f(z)$  models attenuation and amplification along the fiber, and ideal distributed amplification (IDA) has  $f(z) = 1$ . The ASE noise vector  $\mathbf{n}(z, t) = (n(z, t), \bar{n}(z, t))^T$  has entries that are independent Wiener processes in  $z$  such that, in the absence of signal ( $\mathbf{u} = \mathbf{0}$ ) and nonlinearity ( $\gamma = 0$ ), the accumulated noise at a receiver of bandwidth  $\mathcal{B}_{\text{ASE}}$  at  $z = \mathcal{L}$  has two independent components that are Gaussian processes with autocorrelation function  $N_{\text{ASE}} \mathcal{B}_{\text{ASE}} \text{sinc}(\mathcal{B}_{\text{ASE}}(t - t'))$ .

## III. DUAL-POLARIZATION RP MODELS

This section develops simplified models for the Manakov equation. We first derive the continuous-time RP solution of (7). We then consider WDM signaling and develop discrete-time models for dispersion compensation and digital back-propagation (DBP).

RP first solves the Manakov equation without the nonlinear term to obtain  $\mathbf{u}_0(z, t)$  in (12) and then treats the nonlinearity as a small additive term that depends on the linear solution, see (16). As the nonlinear term is cubic and the receiver applies a matched filter, the effect of the nonlinearity depends on the integral over distance and time of the product of four copies of the (time-broadened) base pulse  $s(z, t) = \mathcal{D}_z s(t)$ , see (36). A graphical representation of these four-pulse interactions is given in [26]. The interactions create additive nonlinear interference (NLI) terms that are proportional to the products of three symbols, see (30).

### A. Continuous-Time RP Model

Similar to [15], we expand the signal  $\mathbf{u}$  in powers of  $\gamma$  which is assumed small:

$$\mathbf{u}(z, t) = \mathbf{u}_0(z, t) + \gamma \Delta \mathbf{u}(z, t) + \mathcal{O}(\gamma^2). \quad (8)$$

We substitute (8) in (7), and solve the equations for the zeroth and first powers of  $\gamma$ . The zeroth-order equation is

$$\frac{\partial}{\partial z} \mathbf{u}_0(z, t) = -j \frac{\beta_2}{2} \frac{\partial^2}{\partial t^2} \mathbf{u}_0(z, t) + \frac{1}{\sqrt{f(z)}} \mathbf{n}(z, t). \quad (9)$$

Using the general expression

$$\frac{\partial}{\partial z} (\mathcal{D}_z g(z, t)) = -j \frac{\beta_2}{2} \frac{\partial^2}{\partial t^2} (\mathcal{D}_z g(z, t)) + \mathcal{D}_z \left( \frac{\partial}{\partial z} g(z, t) \right) \quad (10)$$

and choosing

$$g(z, t) = \mathbf{u}(0, t) + \int_0^z \mathcal{D}_{-z'} \frac{\mathbf{n}(z', t)}{f(z')} dz' \quad (11)$$

one can verify that the solution of (9) is

$$\mathbf{u}_0(z, t) = \mathbf{u}_{\text{LIN}}(z, t) + \mathbf{u}_{\text{ASE}}(z, t) \quad (12)$$

where  $\mathbf{u}_{\text{LIN}}(z, t) = \mathcal{D}_z \mathbf{u}(0, t)$  and

$$\mathbf{u}_{\text{ASE}}(z, t) = \mathcal{D}_z \left( \int_0^z \mathcal{D}_{-z'} \frac{\mathbf{n}(z', t)}{f(z')} dz' \right). \quad (13)$$

This is similar to the 1-pol case and the properties derived in [15] apply. The entries  $u_{\text{ASE}}(z, t)$  and  $\bar{u}_{\text{ASE}}(z, t)$  of  $\mathbf{u}_{\text{ASE}}$  are independent, and their autocorrelation functions are

$$\begin{aligned} & \langle u_{\text{ASE}}(z, t) u_{\text{ASE}}^*(z', t') \rangle \\ &= \frac{N_{\text{ASE}}}{\kappa(\mathcal{L}, \mathcal{L})} \kappa(z, z') \mathcal{B}_{\text{ASE}} \text{sinc}(\mathcal{B}_{\text{ASE}}(t - t')) \end{aligned} \quad (14)$$

where

$$\kappa(z, z') = \int_0^{\min\{z, z'\}} \frac{1}{f(z'')} dz'' \quad (15)$$

The first-order equation in  $\gamma$  is

$$\frac{\partial}{\partial z} \Delta \mathbf{u} = -j \frac{\beta_2}{2} \frac{\partial^2}{\partial t^2} \Delta \mathbf{u} + j f(z) \|\mathbf{u}_0\|^2 \mathbf{u}_0. \quad (16)$$

Again applying (10), the solution of (16) is

$$\begin{aligned} \Delta \mathbf{u}(z, t) \\ = j \mathcal{D}_z \left( \int_0^z f(z') \mathcal{D}_{-z'} \left( \|\mathbf{u}_0(z', t)\|^2 \mathbf{u}_0(z', t) \right) dz' \right). \end{aligned} \quad (17)$$

The RP solution of the Manakov equation is thus

$$\mathbf{u}(z, t) = \mathbf{u}_{\text{LIN}}(z, t) + \mathbf{u}_{\text{ASE}}(z, t) + \mathbf{u}_{\text{NL}}(z, t) \quad (18)$$

where  $\mathbf{u}_{\text{NL}}(z, t) = \gamma \Delta \mathbf{u}_0(z, t)$ . The linear and ASE terms are similar to those in the scalar case [15], [22] but  $\mathbf{u}_{\text{NL}}(z, t)$  couples the polarizations via  $\|\mathbf{u}_0(z', t)\|^2$  in (17).

### B. WDM with PAM

We consider pulse amplitude modulation (PAM) with WDM. The WDM channels have indexes  $c$  satisfying

$$c \in \mathcal{C} = \{c_{\min}, \dots, 0, \dots, c_{\max}\} \quad (19)$$

where  $c_{\min} \leq 0$  and  $c_{\max} \geq 0$ . The center angular frequency of channel  $c$  is  $\Omega^{(c)}$ ,  $c \in \mathcal{C}$ , and we choose  $\Omega^{(c)} = 0$ . The two components of the transmitted signal are

$$u(0, t) = \sum_{m=-\infty}^{\infty} x_m s(t - mT) + \sum_{c \neq 0} e^{j\Omega^{(c)}t} \sum_{k=-\infty}^{\infty} b_k^{(c)} s(t - kT - \Delta T^{(c)}) \quad (20)$$

$$\bar{u}(0, t) = \sum_{m=-\infty}^{\infty} \bar{x}_m s(t - mT - \overline{\Delta T}) + \sum_{c \neq 0} e^{j\Omega^{(c)}t} \sum_{k=-\infty}^{\infty} \bar{b}_k^{(c)} s(t - kT - \overline{\Delta T}^{(c)}) \quad (21)$$

where  $T$  is the symbol period and  $s(t)$  is the base pulse that is taken to be the same for all channels. The delays  $\overline{\Delta T}$ ,  $\Delta T^{(c)}$  and  $\overline{\Delta T}^{(c)}$  allow asynchronous transmission. These delays are here measured with respect to the first polarization of the channel of interest (COI) with  $c = 0$ , i.e.,  $\Delta T = \Delta T^{(0)} = 0$ . The symbols transmitted in the COI are  $x_m$  for the first polarization and  $\bar{x}_m$  for the second. The symbols transmitted in the interfering channels are  $b_k^{(c)}$  and  $\bar{b}_k^{(c)}$ .

The base pulse is chosen as a root-Nyquist pulse with unit energy,  $\|s(t)\|^2 = 1$ , with most of its energy in the frequency band  $|\Omega| \leq \pi\mathcal{B}$ . We assume  $2\pi\mathcal{B} \leq \min_c (\Omega^{(c+1)} - \Omega^{(c)})$  so that the channels can be separated in frequency. The transmitted symbol sequences  $\{X_m\}$ ,  $\{\bar{X}_m\}$ ,  $\{B_k^{(c)}\}$  and  $\{\bar{B}_k^{(c)}\}$  are independent and identically distributed (i.i.d.) proper complex processes. The energies are  $\langle |X_m|^2 \rangle = E$  and  $\langle |B_k^{(c)}|^2 \rangle = E^{(c)}$ , and similarly for  $\bar{E}$  and  $\bar{E}^{(c)}$ . The launch power of the first polarization of the COI is thus  $\mathcal{P} = E/T$ . We define the fourth moments  $Q^{(c)} = \langle |B_k^{(c)}|^4 \rangle$  and  $\bar{Q}^{(c)} = \langle |\bar{B}_k^{(c)}|^4 \rangle$ .

We focus on the received symbols in the first polarization. All results apply to the second polarization by letting the variables with ‘‘bar’’ denote the first polarization and the variables without ‘‘bar’’ denote the second.

The receiver uses a band-pass filter  $h_B(t)$  to isolate the COI. We assume that  $h_B(t) * s(t) = s(t)$ . The receiver then applies either dispersion compensation  $\mathcal{D}_{-L}$  or 2-pol digital back-propagation (DBP) to the COI, followed by matched filtering and sampling for each polarization. We proceed to develop discrete-time models for both cases.

### C. Discrete-Time Model for Dispersion Compensation

For dispersion compensation the sampled symbols of the first polarization of the COI are the inner products

$$y_m = \int_{-\infty}^{\infty} s(t - mT)^* \{\mathcal{D}_{-L}[h_B(t) * u(\mathcal{L}, t)]\} dt. \quad (22)$$

where  $*$  denotes convolution. Inserting (18) into (22), we have

$$y_m = x_m + w_m + \Delta x_m \quad (23)$$

where the linear noise term is

$$w_m = \int_{-\infty}^{\infty} s(t - mT)^* \{\mathcal{D}_{-L}[h_B(t) * u_{\text{ASE}}(\mathcal{L}, t)]\} dt. \quad (24)$$

The  $\mathcal{D}_{-L}$  operator does not change the statistical properties of the noise [15]. If most of the energy of  $s(t)$  is contained in the COI with bandwidth  $\mathcal{B}$ , then the  $\{W_m\}$  are i.i.d. proper complex Gaussian with

$$\langle W_m W_{m'}^* \rangle = N_{\text{ASE}} \delta[m' - m] \quad (25)$$

where  $\delta[\ell] = 1$  if  $\ell = 0$  and  $\delta[\ell] = 0$  otherwise. The  $W_m$  are uncorrelated with the  $\bar{W}_m$ .

The NLI term  $\Delta x_m$  is

$$\Delta x_m = \int_{-\infty}^{\infty} s(t - mT)^* \{\mathcal{D}_{-L}[h_B(t) * u_{\text{NL}}(\mathcal{L}, t)]\} dt. \quad (26)$$

As cross-phase modulation (XPM) limits the capacity [8], we neglect signal-noise mixing by replacing  $\mathbf{u}_0$  with  $\mathbf{u}_{\text{LIN}}$  in (17). Substituting the resulting  $u_{\text{NL}}(\mathcal{L}, t)$  into (26) and using the linearity of the  $\mathcal{D}_z$  and  $*$  operators, the dispersion operators  $\mathcal{D}_{-L}$  and  $\mathcal{D}_L$  cancel, and (5) gives

$$\int_{-\infty}^{\infty} s(t)^* \{h_B(t) * [\mathcal{D}_{-z} v(t)]\} dt = \int_{-\infty}^{\infty} \{\mathcal{D}_z[h_B(-t)^* * s(t)]\}^* v(t) dt. \quad (27)$$

We now assume that  $h_B(-t)^* = h_B(t)$ , and use  $h_B(t) * s(t) = s(t)$ . We write  $s(z, t) = \mathcal{D}_z s(t)$  to obtain

$$\Delta x_m = j\gamma \int_0^{\mathcal{L}} f(z) \int_{-\infty}^{\infty} s(z, t - mT)^* \cdot \left( |u_{\text{LIN}}(z, t)|^2 + |\bar{u}_{\text{LIN}}(z, t)|^2 \right) u_{\text{LIN}}(z, t) dt dz. \quad (28)$$

We next insert the WDM signals (20) and (21) into (28) and use the following identity for a delayed and frequency-shifted pulse  $s(t)$ :

$$\mathcal{D}_z \left[ e^{j\Omega^{(c)}t} s(t - t_0) \right] = e^{j\frac{\beta_2}{2}(\Omega^{(c)})^2 z} e^{j\Omega^{(c)}t} s(z, t - t_0 + \beta_2 \Omega^{(c)} z). \quad (29)$$

Ignoring the four-wave mixing (FWM) terms, we obtain

$$\begin{aligned} \Delta x_m = & j \sum_{\substack{n \\ k, k'}} S_{n, k, k'} x_{n+m} x_{k+m} x_{k'+m}^* \\ & + j \sum_{\substack{n \\ k, k'}} \tilde{S}_{n, k, k'} x_{n+m} \bar{x}_{k+m} \bar{x}_{k'+m}^* \\ & + j \sum_{c \neq 0} \sum_{\substack{n \\ k, k'}} C_{n, k, k'}^{(c)} x_{n+m} b_{k+m}^{(c)} b_{k'+m}^{(c)*} \\ & + j \sum_{c \neq 0} \sum_{\substack{n \\ k, k'}} \tilde{C}_{n, k, k'}^{(c)} x_{n+m} \bar{b}_{k+m}^{(c)} \bar{b}_{k'+m}^{(c)*} \\ & + j \sum_{c \neq 0} \sum_{\substack{n \\ k, k'}} D_{n, k, k'}^{(c)} \bar{x}_{n+m} b_{k+m}^{(c)} \bar{b}_{k'+m}^{(c)*}. \end{aligned} \quad (30)$$

We explain the terms of (30) in Sec. III-E below.

#### D. Discrete-Time Model for DBP

For DBP the received signal  $\mathbf{u}(\mathcal{L}, t)$  in (18) is filtered with  $h_B(t)$  and propagated for distance  $\mathcal{L}$  with  $\beta_2$  and  $\gamma$  replaced by  $-\beta_2$  and  $-\gamma$ , respectively, and  $f(z)$  replaced by  $f(\mathcal{L} - z)$ . Again using RP, the DBP signal at distance  $z$  (or overall distance  $\mathcal{L} + z$ ) is as in (18) but without the noise term:

$$\mathbf{u}_{\text{DBP}}(z, t) = \tilde{\mathbf{u}}_{\text{LIN}}(z, t) + \tilde{\mathbf{u}}_{\text{NL}}(z, t) \quad (31)$$

where

$$\tilde{\mathbf{u}}_{\text{LIN}}(z, t) = \mathcal{D}_{-z} [h_B(t) * \mathbf{u}(\mathcal{L}, t)] \quad (32)$$

is the dispersion compensation output and

$$\tilde{\mathbf{u}}_{\text{NL}}(z, t) = -j\gamma \mathcal{D}_{-z} \left( \int_0^z f(\mathcal{L} - z') \cdot \mathcal{D}_{z'} \left( \left\| \tilde{\mathbf{u}}_{\text{LIN}}(z', t) \right\|^2 \tilde{\mathbf{u}}_{\text{LIN}}(z', t) \right) dz' \right). \quad (33)$$

is a nonlinear correction term (see (17) and (18)).

We proceed to simplify (33). Recall from (18) that

$$\mathbf{u}(\mathcal{L}, t) = \mathcal{D}_{\mathcal{L}} \mathbf{u}(0, t) + \mathbf{u}_{\text{ASE}}(\mathcal{L}, t) + \mathbf{u}_{\text{NL}}(\mathcal{L}, t). \quad (34)$$

We now modify  $\tilde{\mathbf{u}}_{\text{LIN}}(z', t)$  in (33) by neglecting the ASE term  $\mathbf{u}_{\text{ASE}}(\mathcal{L}, t)$  and the NLI term  $\mathbf{u}_{\text{NL}}(\mathcal{L}, t)$ . One may justify removing the ASE term as neglecting signal-noise mixing, and the NLI term because it has  $\gamma^2$  or smaller terms only. The correction (33) at  $z = \mathcal{L}$  is thus

$$-j\gamma \int_0^{\mathcal{L}} f(z) \mathcal{D}_{-z} \left( \left\| \mathcal{D}_z \mathbf{u}^{(0)}(0, t) \right\|^2 \mathcal{D}_z \mathbf{u}^{(0)}(0, t) \right) dz \quad (35)$$

where we have applied a change of variables to the integration and written the COI launch signal as  $\mathbf{u}^{(0)}(0, t) = h_B(t) * \mathbf{u}(0, t)$ . The correction term (35) followed by matched filtering and sampling gives (28) but with negative  $\gamma$  and where  $\mathbf{u}_{\text{LIN}}(z, t)$  has only the contributions of the COI. DBP thus gives (30) but without the sums with  $S_{n,k,k'}$  and  $\tilde{S}_{n,k,k'}$ . In other words, the analysis confirms the intuition that, under RP approximation, DBP exactly compensates the intra-channel nonlinearity and does not change inter-channel nonlinearities with respect to dispersion compensation.

#### E. Nonlinear Coefficients

The NLI coefficients in (30) can be expressed using the following general form:

$$A_{n,k,k'}(t_1, t_2, t_3) = \gamma \int_0^{\mathcal{L}} f(z) \int_{-\infty}^{\infty} s(z, t)^* s(z, t - nT - t_1) \cdot s(z, t - kT - t_2) s(z, t - k'T - t_3)^* dt dz. \quad (36)$$

1) *Self-Phase Modulation (SPM)*: As shown above, the SPM terms are present if the receiver uses dispersion compensation but not DBP on the COI. The *self-polarization SPM* terms represent interactions of four pulses from the first polarization (1st-pol) of the COI:

$$jS_{n,k,k'} x_{n+m} x_{k+m} x_{k'+m}^* \quad (37)$$

TABLE I  
SYSTEM PARAMETERS

Parameter	Symbol	Value
Attenuation coefficient	$\alpha$	0.2 dB/km
Dispersion coefficient	$\beta_2$	-21.7 ps <sup>2</sup> /km
Nonlinear coefficient	$\gamma$	1.27 W <sup>-1</sup> km <sup>-1</sup>
Phonon occupancy factor	$\eta$	1
Transmit pulse shape	$s(t)$	sinc
Channel bandwidth	$\mathcal{B}$	50 GHz
Channel spacing	$\Omega^{(1)}/(2\pi)$	50 GHz

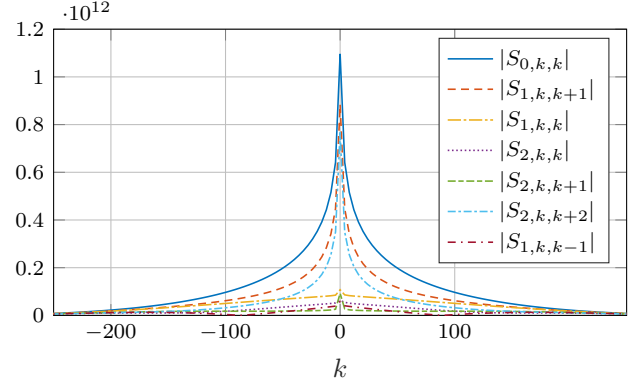


Fig. 1. SPM coefficient magnitudes  $|S_{n,k,k'}|$  for a 1000-km link with the parameters in Table I in the time-synchronized case, where  $S_{n,k,k'} = \tilde{S}_{n,k,k'}$ .

the *cross-polarization SPM* terms represent interactions of two pulses from the 1st-pol of the COI and two pulses from the 2nd-pol of the COI:

$$j\tilde{S}_{n,k,k'} x_{n+m} \bar{x}_{k+m} \bar{x}_{k'+m}^* \quad (38)$$

the SPM coefficients are

$$S_{n,k,k'} = A_{n,k,k'}(0, 0, 0) \quad (39)$$

$$\tilde{S}_{n,k,k'} = A_{n,k,k'}(0, \overline{\Delta T}, \overline{\Delta T}). \quad (40)$$

Fig. 1 shows the  $|S_{n,k,k'}|$  for the parameters in Table I and with synchronized polarizations ( $\overline{\Delta T} = 0$ ). As shown in [11], the coefficients with  $k' = n + k$  are larger than the others.

2) *Cross-Phase Modulation (XPM)*: XPM gives the strongest NLI terms at the capacity peak for systems with DBP of the COI. For all  $c \neq 0$ , the *self-polarization XPM* terms represent interactions of two pulses from the 1st-pol of the COI and two pulses from the 1st-pol of an interfering channel (IC):

$$jC_{n,k,k'}^{(c)} x_{n+m} b_{k+m}^{(c)} b_{k'+m}^{(c)*} \quad (41)$$

the *cross-polarization XPM* terms represent interactions of two pulses from the 1st-pol of the COI and two pulses from the 2nd-pol of an IC:

$$j\tilde{C}_{n,k,k'}^{(c)} x_{n+m} \bar{b}_{k+m}^{(c)} \bar{b}_{k'+m}^{(c)*} \quad (42)$$

and the *mixed-polarization XPM* terms represent interactions of one pulse from the 1st-pol of the COI, one from the 2nd-pol of the COI, one from the 1st-pol of an IC, and one from the 2nd-pol of an IC:

$$jD_{n,k,k'}^{(c)} \bar{x}_{n+m} b_{k+m}^{(c)} \bar{b}_{k'+m}^{(c)*} \quad (43)$$



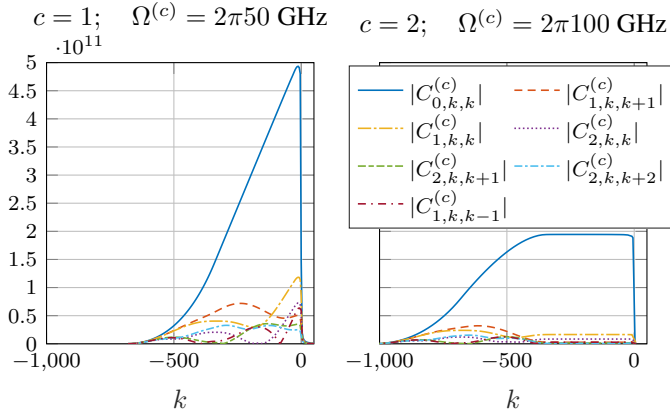


Fig. 2. XPM coefficient magnitudes  $|C_{n,k,k'}^{(c)}|$  for a 1000-km link with the parameters in Table I for the time-synchronized case, where  $C_{n,k,k'}^{(c)} = 2\tilde{C}_{n,k,k'}^{(c)} = 2D_{n,k,k'}^{(c)}$ .

the XPM coefficients are

$$C_{n,k,k'}^{(c)} = 2A_{n,k,k'} \left( 0, \Delta T^{(c)} - \beta_2 \Omega^{(c)} z, \Delta T^{(c)} - \beta_2 \Omega^{(c)} z \right) \quad (44)$$

$$\tilde{C}_{n,k,k'}^{(c)} = A_{n,k,k'} \left( 0, \overline{\Delta T}^{(c)} - \beta_2 \Omega^{(c)} z, \overline{\Delta T}^{(c)} - \beta_2 \Omega^{(c)} z \right) \quad (45)$$

$$D_{n,k,k'} = A_{n,k,k'} \left( \overline{\Delta T}, \Delta T^{(c)} - \beta_2 \Omega^{(c)} z, \overline{\Delta T}^{(c)} - \beta_2 \Omega^{(c)} z \right). \quad (46)$$

All other terms involving only channels 0 and  $c$ , such as  $b_{k'}^{(c)} \bar{b}_k^{(c)} \bar{x}_{k'}^*$  vanish because the  $e^{j\Omega^{(c)}t}$  in (28) do not cancel, and the terms fall outside the receiver filter bandwidth.

We focus on the synchronized case ( $\Delta T^{(c)} = \overline{\Delta T}^{(c)}$  for all  $c$ ) which gives the highest rates in our simulations. We then have  $C_{n,k,k'}^{(c)} = 2\tilde{C}_{n,k,k'}^{(c)} = 2D_{n,k,k'}^{(c)}$ . Fig. 2 shows that the NLI from channel  $c = 2$  has smaller magnitude but longer memory than the NLI from channel  $c = 1$ .

In the synchronized case, we have

$$D_{n,k,k'}^{(c)} = D_{-n,k'-n,k-n}^{(c),*} \quad (47)$$

If  $s(t) = s(-t)$ , we additionally have

$$D_{n,k,k'}^{(c)} = D_{k'-k,k'-n,k'}^{(c)} \quad (48)$$

If  $s(t) = s(-t)$  and  $\Omega^{(-c)} = -\Omega^{(c)}$ , we also have

$$D_{n,k,k'}^{(c)} = D_{-n,-k,-k'}^{(-c)} \quad (49)$$

Equations (47)-(49) similarly hold for the other NLI coefficients  $S_{n,k,k'}$ ,  $\tilde{S}_{n,k,k'}$ ,  $C_{n,k,k'}$  and  $\tilde{C}_{n,k,k'}$ .

#### IV. 2PCPAN MODEL

We consider DBP on the COI and thus neglect the SPM terms. As for the 1-pol case in [22], we separate (30) into terms that depend on the current 2-pol symbol  $\mathbf{x}_m = (x_m, \bar{x}_m)^T$  and those that do not:

$$\begin{pmatrix} \Delta x_m \\ \Delta \bar{x}_m \end{pmatrix} = j \begin{pmatrix} \theta_m & \psi_m \\ \psi_m^* & \bar{\theta}_m \end{pmatrix} \begin{pmatrix} x_m \\ \bar{x}_m \end{pmatrix} + \begin{pmatrix} v_m \\ \bar{v}_m \end{pmatrix} \quad (50)$$

where we have defined

$$\theta_m = \sum_{c \neq 0} \sum_{k,k'} C_{0,k,k'}^{(c)} b_{k+m}^{(c)} b_{k'+m}^{(c),*} + \sum_{c \neq 0} \sum_{k,k'} \tilde{C}_{0,k,k'}^{(c)} \bar{b}_{k+m}^{(c)} \bar{b}_{k'+m}^{(c),*} \quad (51)$$

$$\psi_m = \sum_{c \neq 0} \sum_{k,k'} D_{0,k,k'}^{(c)} b_{k+m}^{(c)} \bar{b}_{k'+m}^{(c),*} \quad (52)$$

$$v_m = j \sum_{c \neq 0} \sum_{n \neq 0} C_{n,k,k'}^{(c)} x_{n+m} b_{k+m}^{(c)} b_{k'+m}^{(c),*} + j \sum_{c \neq 0} \sum_{n \neq 0} \tilde{C}_{n,k,k'}^{(c)} x_{n+m} \bar{b}_{k+m}^{(c)} \bar{b}_{k'+m}^{(c),*} + j \sum_{c \neq 0} \sum_{n \neq 0} D_{n,k,k'}^{(c)} \bar{x}_{n+m} b_{k+m}^{(c)} \bar{b}_{k'+m}^{(c),*} \quad (53)$$

and  $\bar{\theta}_m$ ,  $\bar{\psi}_m$ , and  $\bar{v}_m$  are obtained by swapping  $x_\ell$  with  $\bar{x}_\ell$  and  $b_\ell^{(c)}$  with  $\bar{b}_\ell^{(c)}$  in (51)-(53). From (44) and (45), we have  $C_{0,k,k'}^{(c)} = C_{0,k',k}^{(c),*}$  and  $\tilde{C}_{0,k,k'}^{(c)} = \tilde{C}_{0,k',k}^{(c),*}$ . Therefore,  $\theta_m$  and  $\bar{\theta}_m$  are real.

With  $\Delta T^{(c)} = \overline{\Delta T}^{(c)}$  for all  $c$ , from (47) we have  $D_{0,k,k'}^{(c),*} = D_{0,k',k}^{(c)}$  and therefore

$$\bar{\psi}_m = \psi_m^*. \quad (54)$$

We now apply the following approximation valid to first order in  $\gamma$ :

$$\mathbf{I} + j \begin{pmatrix} \theta_m & \psi_m \\ \psi_m^* & \bar{\theta}_m \end{pmatrix} \approx \exp \left[ j \underbrace{\begin{pmatrix} \theta_m & \psi_m \\ \psi_m^* & \bar{\theta}_m \end{pmatrix}}_{\mathbf{M}_m} \right]. \quad (55)$$

The motivation for the approximation is that both the analytical form of the Manakov equation and numerical results suggest a unitary rotation in two-dimensional (2D) complex space. Note that  $\mathbf{M}_m$  in (55) has the general form of such a rotation where the matrix argument of the exponential is skew-Hermitian. A unitary rotation also simplifies computing the output entropy in Section VI-A. Substituting (50) in (23), and using (55), we obtain the 2pCPAN model of the 2-pol optical channel:

$$\begin{pmatrix} y_m \\ \bar{y}_m \end{pmatrix} = \mathbf{M}_m \begin{pmatrix} x_m \\ \bar{x}_m \end{pmatrix} + \begin{pmatrix} w_m \\ \bar{w}_m \end{pmatrix} + \begin{pmatrix} v_m \\ \bar{v}_m \end{pmatrix} \quad (56)$$

where the  $W_m$  and the  $\bar{W}_m$  are i.i.d. proper complex Gaussian with variance  $N_{\text{ASE}}$ . The matrix  $\mathbf{M}_m$  in (55) represents the NLI that causes a complex 2D rotation of the transmitted symbols, and the  $v_m$  and  $\bar{v}_m$  are the residual NLI that is not captured by  $\mathbf{M}_m$ . The  $\theta_m$  and  $\bar{\theta}_m$  in  $\mathbf{M}_m$  represent phase noise in each polarization, and  $\psi_m$  represents a unitary coupling between polarizations.

#### A. First- and Second-Order Statistics

We compute statistics of  $\{\Theta_m\}$ ,  $\{\Psi_m\}$ , and  $\{V_m\}$ . The statistics of  $\{\bar{\Theta}_m\}$  and  $\{\bar{V}_m\}$  are respectively the same as those for  $\{\Theta_m\}$  and  $\{V_m\}$  after swapping  $E^{(c)}$  and  $Q^{(c)}$  with  $\bar{E}^{(c)}$  and  $\bar{Q}^{(c)}$ , respectively.

1) *Means*: We have

$$\langle \Theta_m \rangle = \sum_{c \neq 0} E^{(c)} \sum_k C_{0,k,k}^{(c)} + \sum_{c \neq 0} \bar{E}^{(c)} \sum_k \tilde{C}_{0,k,k}^{(c)} \quad (57)$$

$$\langle \Psi_m \rangle = \langle V_m \rangle = 0. \quad (58)$$

2) *Second-Order Statistics of  $\Theta_m$* : The autocovariance function of  $\{\Theta_m\}$  is

$$\begin{aligned} r_{\Theta}[\ell] &:= \langle \Theta_m \Theta_{m+\ell} \rangle - \langle \Theta_m \rangle \langle \Theta_{m+\ell} \rangle \\ &= \sum_{c \neq 0} \left( Q^{(c)} - \left( E^{(c)} \right)^2 \right) \sum_k C_{0,k,k}^{(c)} C_{0,k-\ell,k-\ell}^{(c),*} \\ &\quad + \sum_{c \neq 0} \left( E^{(c)} \right)^2 \sum_{k \neq k'} C_{0,k,k'}^{(c)} C_{0,k-\ell,k'-\ell}^{(c),*} \\ &\quad + \sum_{c \neq 0} \left( \bar{Q}^{(c)} - \left( \bar{E}^{(c)} \right)^2 \right) \sum_k \tilde{C}_{0,k,k}^{(c)} \tilde{C}_{0,k-\ell,k-\ell}^{(c),*} \\ &\quad + \sum_{c \neq 0} \left( \bar{E}^{(c)} \right)^2 \sum_{k \neq k'} \tilde{C}_{0,k,k'}^{(c)} \tilde{C}_{0,k-\ell,k'-\ell}^{(c),*}. \end{aligned} \quad (59)$$

The crosscovariance function of  $\{\Theta_m\}$  and  $\{\bar{\Theta}_m\}$  is

$$\begin{aligned} \tilde{r}_{\Theta}[\ell] &:= \langle \Theta_m \bar{\Theta}_{m+\ell} \rangle - \langle \Theta_m \rangle \langle \bar{\Theta}_{m+\ell} \rangle \\ &= \sum_{c \neq 0} \left( Q^{(c)} - \left( E^{(c)} \right)^2 \right) \sum_k C_{0,k,k}^{(c)} \tilde{C}_{0,k-\ell,k-\ell}^{(c),*} \\ &\quad + \sum_{c \neq 0} \left( E^{(c)} \right)^2 \sum_{k \neq k'} C_{0,k,k'}^{(c)} \tilde{C}_{0,k-\ell,k'-\ell}^{(c),*} \\ &\quad + \sum_{c \neq 0} \left( \bar{Q}^{(c)} - \left( \bar{E}^{(c)} \right)^2 \right) \sum_k \tilde{C}_{0,k,k}^{(c)} C_{0,k-\ell,k-\ell}^{(c),*} \\ &\quad + \sum_{c \neq 0} \left( \bar{E}^{(c)} \right)^2 \sum_{k \neq k'} \tilde{C}_{0,k,k'}^{(c)} C_{0,k-\ell,k'-\ell}^{(c),*}. \end{aligned} \quad (60)$$

When  $\Delta T^{(c)} = \overline{\Delta T}^{(c)}$  for all  $c$ , we have  $\tilde{C}_{0,k,k'}^{(c)} = C_{0,k,k'}^{(c)}/2$ . Furthermore, if  $E^{(c)} = \bar{E}^{(c)}$  and  $Q^{(c)} = \bar{Q}^{(c)}$  for all  $c$ , then (59) and (60) simplify to

$$r_{\Theta}[\ell] = r_{\bar{\Theta}}[\ell] = \frac{5}{4} \tilde{r}_{\Theta}[\ell] \quad (61)$$

$$\begin{aligned} \tilde{r}_{\Theta}[\ell] &= \sum_{c \neq 0} \left( Q^{(c)} - \left( E^{(c)} \right)^2 \right) \sum_k C_{0,k,k}^{(c)} C_{0,k-\ell,k-\ell}^{(c),*} \\ &\quad + \left( E^{(c)} \right)^2 \sum_{c \neq 0} \sum_{k \neq k'} C_{0,k,k'}^{(c)} C_{0,k-\ell,k'-\ell}^{(c),*}. \end{aligned} \quad (62)$$

The phase noises across polarizations are thus almost as strongly correlated as within each polarization.

3) *Second-Order Statistics of  $\Psi_m$* : The autocorrelation function of  $\{\Psi_m\}$  is

$$r_{\Psi}[\ell] := \langle \Psi_m \Psi_{m+\ell}^* \rangle = \sum_{c \neq 0} E^{(c)} \bar{E}^{(c)} \sum_{k,k'} D_{0,k,k'}^{(c)} D_{0,k-\ell,k'-\ell}^{(c),*} \quad (63)$$

If  $\Delta T^{(c)} = \overline{\Delta T}^{(c)}$  for all  $c$ , then from (47) we have  $D_{0,k,k'}^{(c)} = D_{0,k',k}^{(c),*}$  and  $r_{\Psi}[\ell]$  is real. If we have Gaussian inputs and if  $E^{(c)} = \bar{E}^{(c)}$  for all  $c$ , then  $Q^{(c)} = 2(E^{(c)})^2$  and

$$r_{\Psi}[\ell] = \frac{1}{5} r_{\Theta}[\ell]. \quad (64)$$

From (52), the  $\{\Psi_m\}$  are proper complex: for all  $\ell$  we have

$$\langle \Psi_m \Psi_{m+\ell} \rangle = 0. \quad (65)$$

4) *Second-Order Statistics of  $V_m$* : The autocorrelation function of  $\{V_m\}$  is given by

$$\begin{aligned} r_V[\ell] &:= \langle V_m V_{m+\ell}^* \rangle \\ &= E \sum_{c \neq 0} \left( Q^{(c)} - \left( E^{(c)} \right)^2 \right) \sum_{\substack{n \neq 0 \\ n \neq \ell}} \sum_k C_{n,k,k}^{(c)} C_{n-\ell,k-\ell,k-\ell}^{(c),*} \\ &\quad + E \sum_{c \neq 0} \left( E^{(c)} \right)^2 \sum_{\substack{n \neq 0 \\ n \neq \ell}} \sum_{k \neq k'} C_{n,k,k'}^{(c)} C_{n-\ell,k-\ell,k'-\ell}^{(c),*} \\ &\quad + E \sum_{c \neq 0} \left( \bar{Q}^{(c)} - \left( \bar{E}^{(c)} \right)^2 \right) \sum_{\substack{n \neq 0 \\ n \neq \ell}} \sum_k \tilde{C}_{n,k,k}^{(c)} \tilde{C}_{n-\ell,k-\ell,k-\ell}^{(c),*} \\ &\quad + E \sum_{c \neq 0} \left( \bar{E}^{(c)} \right)^2 \sum_{\substack{n \neq 0 \\ n \neq \ell}} \sum_{k \neq k'} \tilde{C}_{n,k,k'}^{(c)} \tilde{C}_{n-\ell,k-\ell,k'-\ell}^{(c),*} \\ &\quad + E \sum_{\substack{c \neq 0 \\ c' \neq 0}} E^{(c)} E^{(c')} \sum_{\substack{n \neq 0 \\ n \neq \ell}} \sum_{k,k'} C_{n,k,k}^{(c)} C_{n-\ell,k'-\ell,k'-\ell}^{(c'),*} \\ &\quad + E \sum_{\substack{c \neq 0 \\ c' \neq 0}} \bar{E}^{(c)} \bar{E}^{(c')} \sum_{\substack{n \neq 0 \\ n \neq \ell}} \sum_{k,k'} \tilde{C}_{n,k,k}^{(c)} \tilde{C}_{n-\ell,k'-\ell,k'-\ell}^{(c'),*} \\ &\quad + E \sum_{\substack{c \neq 0 \\ c' \neq 0}} E^{(c)} \bar{E}^{(c')} \sum_{\substack{n \neq 0 \\ n \neq \ell}} \sum_{k,k'} C_{n,k,k}^{(c)} \tilde{C}_{n-\ell,k'-\ell,k'-\ell}^{(c'),*} \\ &\quad + E \sum_{\substack{c \neq 0 \\ c' \neq 0}} \bar{E}^{(c)} E^{(c')} \sum_{\substack{n \neq 0 \\ n \neq \ell}} \sum_{k,k'} \tilde{C}_{n,k,k}^{(c)} C_{n-\ell,k'-\ell,k'-\ell}^{(c'),*} \\ &\quad + \bar{E} \sum_{\substack{c \neq 0 \\ c' \neq 0}} E^{(c)} \bar{E}^{(c')} \sum_{\substack{n \neq 0 \\ n \neq \ell}} \sum_{k,k'} D_{n,k,k'}^{(c)} D_{n-\ell,k'-\ell,k'-\ell}^{(c'),*}. \end{aligned} \quad (66)$$

The crosscorrelation and pseudocorrelations of the  $\{V_m\}$  are:

$$\langle V_m \bar{V}_{m+\ell}^* \rangle = \langle V_m V_{m+\ell} \rangle = \langle V_m \bar{V}_{m+\ell} \rangle = 0. \quad (67)$$

5) *Crosscorrelations*: For all  $m, \ell$ , we have

$$\langle \Psi_m \Theta_{\ell} \rangle = \langle \Psi_m \bar{\Theta}_{\ell} \rangle = 0 \quad (68)$$

$$\langle V_m \Theta_{\ell} \rangle = \langle V_m \bar{\Theta}_{\ell} \rangle = 0 \quad (69)$$

$$\langle \Psi_m V_{\ell}^* \rangle = \langle \Psi_m V_{\ell} \rangle = \langle \Psi_m \bar{V}_{\ell}^* \rangle = \langle \Psi_m \bar{V}_{\ell} \rangle = 0 \quad (70)$$

$$\langle V_m X_m^* \rangle = \langle V_m X_{\ell} \rangle = \langle \bar{V}_m X_m^* \rangle = \langle \bar{V}_m X_{\ell} \rangle = 0 \quad (71)$$

$$\langle \bar{V}_m X_{\ell}^* \rangle = 0 \quad (72)$$

but for  $m \neq \ell$  we also have

$$\begin{aligned} \langle V_m X_{\ell}^* \rangle &= jE \sum_{c \neq 0} E^{(c)} \sum_k C_{\ell-m,k,k}^{(c)} \\ &\quad + jE \sum_{c \neq 0} \bar{E}^{(c)} \sum_k \tilde{C}_{\ell-m,k,k}^{(c)} \end{aligned} \quad (73)$$

so the additive NLI noise  $V_m$  is correlated with the input symbols  $X_m$  of the same polarization. This can be interpreted as inter-symbol interference (ISI).

### B. Large Accumulated Dispersion

The synchronized case has  $C_{n,k,k'}/2 = \tilde{C}_{n,k,k'} = D_{n,k,k'}$ . For IDA,  $E^{(c)} = \bar{E}^{(c)}$  and  $Q^{(c)} = \bar{Q}^{(c)}$  for all  $c$ , the approximations proposed in [16] for large accumulated dispersion can be adapted to the 2-pol case. In other words, if  $|\beta_2\Omega^{(c)}|\mathcal{L}/T \gg 1$  for all  $c \in \mathcal{C} \setminus \{0\}$  then

$$\langle \Theta_m \rangle \approx 3\gamma \frac{\mathcal{L}}{T} \sum_{c \neq 0} E^{(c)} \quad (74)$$

$$r_\Theta[\ell] \approx \frac{5\gamma^2 \mathcal{L}}{T} \sum_{c \neq 0} \frac{Q^{(c)} - (E^{(c)})^2}{|\beta_2\Omega^{(c)}|} \left[ 1 - \frac{|\ell|T}{|\beta_2\Omega^{(c)}|\mathcal{L}} \right]^+ \quad (75)$$

where  $[x]^+ := \max(x, 0)$ . The factors 3 and 5 are different than in [22, Eqs. (49) and (50)] because the mean phase noise is 3/2 times larger than its 1-pol counterpart due to the last summand in (57), and  $r_\Theta[\ell]$  is 5/4 times its 1-pol counterpart due to the last 2 lines in (59). Eqs. (61) and (64) still apply.

## V. SIMPLIFIED MODELS FOR COMPUTATION

In the following, the receiver removes the means  $\langle \Theta_m \rangle$  and  $\langle \bar{\Theta}_m \rangle$  of the phase noise, and we abuse notation and write  $\Theta_m$  and  $\bar{\Theta}_m$  for the resulting zero-mean variables. For each channel  $c$ , both polarizations have the same delay ( $\Delta T^{(c)} = \bar{\Delta T}^{(c)}$ ), energy ( $E^{(c)} = \bar{E}^{(c)}$ ), and fourth moment ( $Q^{(c)} = \bar{Q}^{(c)}$ ). The models can be adapted to cases where these conditions do not hold but the resulting increase in the number of parameters substantially increases the computational cost of the training in Section VI-C.

### A. Polarization Drift (PD) Model

The PD model was proposed in [27] and used in [4] to compute achievable rates of 2-pol systems. Consider the Pauli matrices:

$$\boldsymbol{\sigma}_1 = \begin{pmatrix} 0 & 1 \\ 1 & 0 \end{pmatrix}, \quad \boldsymbol{\sigma}_2 = \begin{pmatrix} 0 & -j \\ j & 0 \end{pmatrix}, \quad \boldsymbol{\sigma}_3 = \begin{pmatrix} 1 & 0 \\ 0 & -1 \end{pmatrix}. \quad (76)$$

An isotropic random rotation on the Poincaré sphere (IRRPS) of  $\mathbf{v}_m \in \mathbb{C}^2$  can be represented as  $\mathbf{z}_m = \mathbf{U}_m \mathbf{v}_m$  where

$$\mathbf{U}_m = \exp[j(\alpha_{1,m}\boldsymbol{\sigma}_1 + \alpha_{2,m}\boldsymbol{\sigma}_2 + \alpha_{3,m}\boldsymbol{\sigma}_3)] \quad (77)$$

and where  $\alpha_{1,m}$ ,  $\alpha_{2,m}$  and  $\alpha_{3,m}$  are i.i.d. real Gaussian with zero mean and variance  $\sigma_A^2$ . An IRRPS is such that the probability density function (PDF) of  $\mathbf{z}_m$  does not change if  $\mathbf{z}_m$  is expressed as a Stokes vector and rotated around  $\mathbf{v}_m$ .

The PD model for (23) is an extension of the Wiener phase noise model for the 1-pol case:

$$\mathbf{y}_m = e^{j\theta_m} \mathbf{J}_m \mathbf{x}_m + \mathbf{w}_m \quad (78)$$

where  $\{\Theta_m\}$  is Wiener phase noise that is common to both polarizations:

$$\theta_m = \theta_{m-1} + \sigma_\Delta \delta_m \quad (79)$$

with the  $\Delta_m$  being i.i.d. standard real Gaussian variables. The  $\{\Theta_m\}$  do not change the polarization state of the signal. The

matrix  $\mathbf{J}_m$  is a random walk over the Poincaré sphere obtained as a cumulative product of IRRPSs of the form (77):

$$\mathbf{J}_m = \mathbf{U}_m \mathbf{J}_{m-1}. \quad (80)$$

The NLI in the PD model has phase noise that converges to a uniform distribution over the Poincaré sphere [27]. This is not what the RP or LP models predict: the matrix  $\mathbf{M}_m$  in (56) has entries that give a distribution with small variance around the transmitted symbol  $\mathbf{x}_m$ . Nonetheless, the PD model gives achievable rates that are very close to those obtained here, see [4] and the simulation results below.

### B. Markov Rotation (MR) Model

The statistical analysis in Section IV-A predicts in (62) that  $\langle \Theta_m \Theta_\ell \rangle = (5/4) \langle \Theta_m \bar{\Theta}_\ell \rangle$ . This can be modeled by choosing  $\theta_m = 2\phi_m + \bar{\phi}_m$  and  $\bar{\theta}_m = 2\bar{\phi}_m + \phi_m$ , where the  $\{\Phi_m\}$  and the  $\{\bar{\Phi}_m\}$  are two independent zero-mean processes with variance  $\langle \Theta_m^2 \rangle / 5$ . We model the NLI rotation  $\mathbf{M}_m$  of (55) as

$$\mathbf{M}_m = \exp \left[ j \begin{pmatrix} 2\phi_m + \bar{\phi}_m & \psi_m \\ \psi_m^* & \phi_m + 2\bar{\phi}_m \end{pmatrix} \right] \quad (81)$$

where the  $\Phi_m$  and  $\bar{\Phi}_m$  are independent real Markov processes with memory  $\mu$  and with the same statistical properties. Similar to what we did in [22], for each  $m$  we model  $(\Phi_{m-\mu}, \dots, \Phi_m)$  as jointly Gaussian with a symmetric Toeplitz covariance matrix  $\mathbf{C}_\mu$  whose first column is  $(r_\Theta[0], \dots, r_\Theta[\mu])^T / 5$ . This Markov approach yields long autocorrelation functions with small memory that replace the functions (59)-(60) from the analytical model. We divide  $\mathbf{C}_\mu$  into four blocks:

$$\mathbf{C}_\mu = \begin{pmatrix} c_{11} & \mathbf{c}_{12}^T \\ \mathbf{c}_{21} & \mathbf{C}_{22} \end{pmatrix} \quad (82)$$

where  $c_{11}$  is a scalar and  $\mathbf{C}_{22}$  has size  $\mu \times \mu$ . As in [22], the update function for  $\phi_m$  is

$$\phi_m = \sum_{p=1}^{\mu} g_p \phi_{m-p} + \sigma_\mu \delta_m \quad (83)$$

where the  $\Delta_m$  are i.i.d. real standard Gaussian, where

$$\mathbf{g}^T = (g_1 \quad \dots \quad g_\mu) = \mathbf{c}_{12}^T \mathbf{C}_{22}^{-1} \quad (84)$$

and where the increment variance  $\sigma_\mu^2$  is

$$\sigma_\mu^2 = c_{11} - \mathbf{g}^T \mathbf{c}_{21}. \quad (85)$$

The  $\{\Psi_m\}$  in (81) is a proper complex Markov process independent of  $\{\Phi_m\}$  and  $\{\bar{\Phi}_m\}$ , as predicted by (68). The vector  $(\Psi_{m-\mu}, \dots, \Psi_m)$  has a conjugate symmetric Toeplitz covariance matrix whose first column is  $(r_\Psi[0], \dots, r_\Psi[\mu])^T$  from (63). The process is generated similar to (83), but now the  $\Delta_m$  are circularly symmetric complex Gaussian (CSCG) with unit variance.

### C. Simplified 2pCPAN Model

As in [22], we combine the ASE noise and the residual NLI noise (53) into one additive noise term  $\mathbf{z}_m = \mathbf{w}_m + \mathbf{v}_m$ . The simplified 2pCPAN model is

$$\mathbf{y}_m = \mathbf{M}_m \mathbf{x}_m + \mathbf{z}_m \quad (86)$$

where  $\mathbf{M}_m$  is given by (81). From (67), the  $Z_m$  are uncorrelated with the  $\bar{Z}_m$ . We model them as two CSCG processes independent of the  $X_m$  and the  $\bar{X}_m$  (i.e., we neglect (73)) with autocorrelation functions

$$r_Z[\ell] := \langle Z_m Z_{m+\ell}^* \rangle = N_{\text{ASE}} \delta[\ell] + r_V[\ell] \quad (87)$$

and  $r_{\bar{Z}}$  defined similarly.

## VI. ACHIEVABLE RATES

The additive noise processes  $\{Z_m\}$  and  $\{\bar{Z}_m\}$  are uncorrelated with each other, and their autocorrelation functions seem to have a very small imaginary part. We thus whiten the noise processes separately for each polarization with real filters  $\mathbf{h}$  and  $\bar{\mathbf{h}}$  with  $L$  taps and unit norm ( $\|\mathbf{h}\| = \|\bar{\mathbf{h}}\| = 1$ ):

$$\begin{aligned} \mathbf{a}_m &= \sum_{\ell=0}^{L-1} \begin{pmatrix} h_\ell & 0 \\ 0 & \bar{h}_\ell \end{pmatrix} \mathbf{y}_{m-\ell} \\ &= \left( \sum_{\ell=0}^{L-1} \begin{pmatrix} h_\ell & 0 \\ 0 & \bar{h}_\ell \end{pmatrix} \mathbf{M}_{m-\ell} \mathbf{x}_{m-\ell} \right) + \begin{pmatrix} \xi_m \\ \bar{\xi}_m \end{pmatrix}. \end{aligned} \quad (88)$$

Our mismatched channel model is (88) with outputs  $\{\mathbf{a}_m\}$ , where  $\mathbf{M}_m$  has the statistics given in Sec. V-B, and the  $\{\xi_m\}$  and  $\{\bar{\xi}_m\}$  are i.i.d. CSCG processes with variance  $\sigma_\Xi^2$  estimated from training data.

As in [22], we obtain a lower bound on the achievable rate of the Manakov channel via

$$I_q(\mathbf{X}; \mathbf{A}) = h_q(\mathbf{A}) - h_q(\mathbf{A}|\mathbf{X}) \quad (89)$$

where  $\mathbf{X}$  represents the two blocks of symbols  $(X_1, \dots, X_M)$  and  $(\bar{X}_1, \dots, \bar{X}_M)$ , while  $\mathbf{A}$  represents  $(A_1, \dots, A_M)$   $(\bar{A}_1, \dots, \bar{A}_M)$ . We define

$$h_q(\mathbf{A}) = -\langle \log_2 q_{\mathbf{A}}(\mathbf{A}) \rangle. \quad (90)$$

and similarly for  $h_q(\mathbf{A}|\mathbf{X})$ . Here  $q_{\mathbf{A}|\mathbf{X}}(\cdot)$  is the conditional distribution of the channel (88), and  $q_{\mathbf{A}}(\mathbf{a}) = \int_{\mathbf{X}} p_{\mathbf{X}}(\mathbf{x}) q_{\mathbf{A}|\mathbf{X}}(\mathbf{a}|\mathbf{x}) d\mathbf{x}$  where  $p_{\mathbf{X}}(\cdot)$  is the density of the input symbols  $\mathbf{X}$ . We choose the  $\mathbf{X}$  to be i.i.d. CSCG with variance  $E = \mathcal{P}T$ . The expectation in (90) is computed by Monte Carlo simulations and averaging over the channel realizations.

### A. Mismatched Output Entropy $h_q(\mathbf{A})$

Let  $\mathbf{a} = (a_1, \dots, a_M)^T$  and  $\bar{\mathbf{a}} = (\bar{a}_1, \dots, \bar{a}_M)^T$  be two blocks of simulated channel outputs. As  $\mathbf{M}_m$  is unitary, the components of  $\{\mathbf{M}_m \mathbf{x}_m\}$  are i.i.d. CSCG with variance  $E$ . This lets us separate the two polarizations. From (88) we have

$$q_{\mathbf{A}}(\mathbf{a}) = \frac{\exp\left(-\mathbf{a}^H \mathbf{R}_{\mathbf{A}}^{-1} \mathbf{a}\right)}{\det\left(\pi \mathbf{R}_{\mathbf{A}}\right)} \quad (91)$$

where  $\mathbf{R}_{\mathbf{A}}$  is a covariance matrix whose first column is  $(r_{\mathbf{A}}[0], \dots, r_{\mathbf{A}}[M-1])^T$  where

$$r_{\mathbf{A}}[\ell] := \langle A_m A_{m+\ell}^* \rangle = E \sum_{k=0}^{L-1} h_k h_{k+\ell}^* + \sigma_\Xi^2 \delta[\ell]. \quad (92)$$

We set  $h_\ell = 0$  for  $\ell \notin \{0, \dots, L-1\}$ . The mismatched output entropy is approximated as

$$h_q(\mathbf{A}) = -\log_2 q_{\mathbf{A}}(\mathbf{a}) - \log_2 q_{\bar{\mathbf{A}}}(\bar{\mathbf{a}}). \quad (93)$$

We estimate  $h_q(\mathbf{A})$  by averaging (93) over  $N$  simulation runs.

### B. Mismatched Conditional Entropy $h_q(\mathbf{A}|\mathbf{X})$

We use particle filtering [22] to estimate  $h_q(\mathbf{A}|\mathbf{X})$ . The method tracks the parameters  $\phi_m$ ,  $\bar{\phi}_m$  and  $\psi_m$  using a list of  $K$  particles. After processing  $\mathbf{a}_{m-1}$ , the  $k$ -th particle is a 4-tuple with a *weight*  $W_{m-1}^{(k)}$  and three realizations of the parameters of  $\mathbf{M}_{m-1}$ , namely a vector  $(\phi_{m-\mu}^{(k)}, \dots, \phi_{m-1}^{(k)})$ , a vector  $(\bar{\phi}_{m-\mu}^{(k)}, \dots, \bar{\phi}_{m-1}^{(k)})$  and a vector  $(\psi_{m-\mu}^{(k)}, \dots, \psi_{m-1}^{(k)})$ . The  $K$  weights sum to 1. At the  $m$ -th iteration, the three realizations of each particle are updated using (83) and the corresponding equation for  $\Psi_m$ . Let  $p_{\Xi}(\cdot)$  be the PDF of a two-component CSCG variable with variance  $\sigma_\Xi^2$ . The quantity

$$D_m = \sum_{k=1}^K W_{m-1}^{(k)} p_{\Xi} \left( \mathbf{a}_m - \sum_{\ell=0}^{L-1} \begin{pmatrix} h_\ell & 0 \\ 0 & \bar{h}_\ell \end{pmatrix} \mathbf{M}_{m-\ell}^{(k)} \mathbf{x}_{m-\ell} \right) \quad (94)$$

gives an estimate of  $q(\mathbf{a}_m | \mathbf{a}_1, \dots, \mathbf{a}_{m-1}, \mathbf{x}_1, \dots, \mathbf{x}_M)$ . The weights are updated in a manner similar to [22, Eq. (70)]:

$$W_m^{(k)} = \frac{W_{m-1}^{(k)}}{D_m} p_{\Xi} \left( \mathbf{a}_m - \sum_{\ell=0}^{L-1} \begin{pmatrix} h_\ell & 0 \\ 0 & \bar{h}_\ell \end{pmatrix} \mathbf{M}_{m-\ell}^{(k)} \mathbf{x}_{m-\ell} \right). \quad (95)$$

After the update (95), resampling [22] is applied if necessary. After the last iteration, the mismatched conditional entropy is estimated as

$$h_q(\mathbf{A}|\mathbf{X}) = -\sum_{m=1}^M \log_2 D_m. \quad (96)$$

We refine the estimate of  $h_q(\mathbf{A}|\mathbf{X})$  by averaging (96) over  $N$  simulation runs. We then use (89) to lower bound the capacity.

### C. Estimating Model Parameters

The parameters of the 2pCPAN model are computed from training data as in [22]. Similar to [4], we estimate  $\sigma_\Xi^2$  by neglecting the small correlations in  $\{Z_m\}$  and  $\{\bar{Z}_m\}$ , and by approximating  $\|\mathbf{Y}_m\|^2 \|\mathbf{X}_m\|^2$  as being independent with a noncentral chi-squared distribution with four degrees of freedom. More precisely, we estimate  $\sigma_\Xi^2$  as

$$\begin{aligned} \hat{\sigma}_\Xi^2 &= \arg \max_{\sigma^2} \\ &\sum_{m=1}^M \log \left[ \frac{1}{\sigma^2} e^{-\frac{\|\mathbf{y}_m\|^2 + \|\mathbf{x}_m\|^2}{\sigma^2}} \frac{\|\mathbf{y}_m\|}{\|\mathbf{x}_m\|} I_1 \left( \frac{2\|\mathbf{y}_m\| \|\mathbf{x}_m\|}{\sigma^2} \right) \right]. \end{aligned} \quad (97)$$



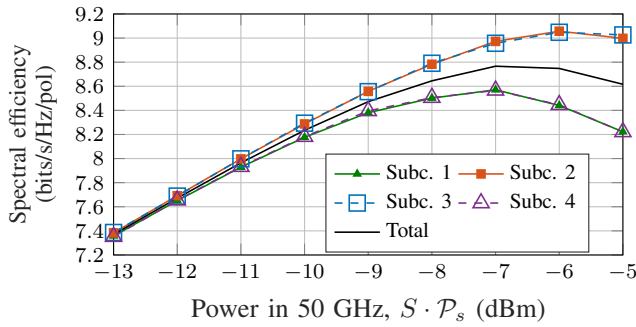


Fig. 3. Spectral efficiency per subcarrier (Subc.) for a 1000-km link with uniform power allocation, synchronized channels, and the parameters in Table I.

where  $I_1(\cdot)$  is the modified Bessel function of the first kind of order one. We estimate the mean phase noise  $\langle \Theta_m \rangle$  as

$$\langle \hat{\Theta}_m \rangle = \text{angle} \left( \frac{1}{M} \sum_{m=1}^M y_m x_m^* \right). \quad (98)$$

For the MR model with (81), we assume that  $r_\Phi[\ell] = r_{\bar{\Phi}}[\ell]$  and that both autocovariance functions are proportional to (75). We also assume that  $r_\Psi[\ell]$  is proportional to (75). We then minimize  $h_q(\mathbf{Y}|\mathbf{X})$  (computed using particle filtering) over the two scaling factors. Finally, the whitening filters  $\mathbf{h}$  and  $\bar{\mathbf{h}}$  are chosen to be real, symmetric, equal, and with a length of  $L = 3$  taps per polarization. This leaves one real degree of freedom:  $h_2 = \bar{h}_2$ . We minimize  $h_q(\mathbf{A}|\mathbf{X})$  over  $h_2$ .

## VII. MULTI-CARRIER COMMUNICATION

The second-order statistics of  $\{\Theta_m\}$ ,  $\{\bar{\Theta}_m\}$ ,  $\{\Psi_m\}$  depend on the difference in frequency to the closest interfering channel [4], [22], and this observation motivates multi-carrier signaling [4]. Suppose each channel  $c$  has  $S$  subcarriers with bandwidth  $B/S$  and the subcarriers are back-propagated jointly at the receiver. We again use FDPA and apply power  $\mathcal{P}_s$  to subcarrier  $s$  for  $s \in \{1, \dots, S\}$ , see [22]. We here use the same heuristic to choose the powers as in [22]:

$$\arg \max_{(\mathcal{P}_1, \dots, \mathcal{P}_S)} \sum_{s=1}^S \text{rate}_s(\mathcal{P}_s) \text{ s.t. } \sum_{s=1}^S \mathcal{P}_s = \mathcal{P} \quad (99)$$

where  $\text{rate}_s(\mathcal{P}_s)$  is the rate of subcarrier  $s$  with uniform power allocation and subcarrier power  $\mathcal{P}_s$ . The functions  $\text{rate}_s(\cdot)$  are approximated by linear interpolation between simulated operating points at intervals of 1 dBm, as shown in Fig. 3. The power allocation from (99) gives curves  $\text{rate}_s(\cdot)$  that are used to optimize the powers in an iterative fashion. The results in Fig. 4 use one iteration of (99).

## VIII. NUMERICAL RESULTS

We simulate single-carrier and four-subcarrier (4SC) systems over a 1000-km fiber with the parameters in Table I. The input distribution is i.i.d. Gaussian. The receiver uses a band-pass filter of bandwidth 50 GHz to isolate the COL, and then applies DBP jointly to  $S$  subcarriers, followed by  $S$  matched filters, and  $S$  particle filters.

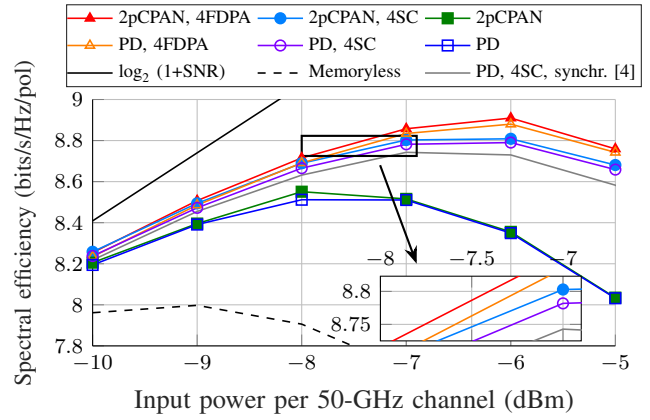


Fig. 4. Spectral efficiency for a 2-pol 1000-km link with the parameters in Table I and the frequency-dependent delays given by (100) and (101). The curve “PD,4SC,synchr.” has all delays equal to 0 and uses the same scheme as the best curve from [4, Fig. 3(a)].

### A. Dual Polarization System

In the 2-pol single-carrier system, we transmit 24 training sequences to estimate the parameters of the PD and 2pCPAN models according to Sec. VI-C.  $N = 120$  testing sequences are then used to compute achievable rates as explained in Sec. VI. The sequence length is  $M = 6825$  symbols per WDM channel. In the 4SC system, the sequence length per subcarrier is  $M = 2047$  symbols, and there are 20 training sequences and  $N = 100$  testing sequences.

Frequency-dependent delays, but with  $\Delta T^{(c)} = \bar{\Delta} T^{(c)}$  for all  $c$ , increase the rates with respect to the fully synchronized case. We chose the single-carrier delays as

$$\begin{aligned} \Delta \mathbf{T} &= \left( \Delta T^{(-2)}, \Delta T^{(-1)}, \Delta T^{(0)}, \Delta T^{(1)}, \Delta T^{(2)} \right) \\ &= (5, 6, -6, 6, 2) \frac{T}{15}. \end{aligned} \quad (100)$$

and the 4-subcarrier (4SC) delays as

$$\begin{aligned} \Delta \mathbf{T}_{4SC} &= \left( (-25, -14, 2, 27), (27, -21, 28, 27), (-1, 18, \right. \\ &\quad \left. -22, -5), (24, 17, 27, 9), (-28, 20, 26, 10) \right) \frac{T_{4SC}}{60} \end{aligned} \quad (101)$$

where  $T_{4SC} = 4T$ . These delays were chosen randomly and optimization could increase the rates further. Note that here  $\Delta T^{(0)} \neq 0$ .

The spectral efficiencies are plotted in Fig. 4. The peak rate of the 4SC system with FDPA (4FDPA) using 2pCPAN is 8.91 bits/s/Hz/pol at -6 dBm. The 2pCPAN 4FDPA system provides a gain of 0.17 bits/s/Hz/pol or 0.8 dB with respect to our implementation of the system in [4] (PD, 4SC, same delays) at its peak rate. Starting with the system in [4], frequency-dependent delays add 0.05 bits/s/Hz/pol, and FDPA adds another 0.09 bits/s/Hz/pol. Replacing the PD receiver with the MR receiver (without the whitening filter, not shown in Fig. 4) adds 0.015 bits/s/Hz/pol, and adding the whitening filter (88) adds another 0.015 bits/s/Hz/pol, yielding the 2pCPAN, 4FDPA curve.

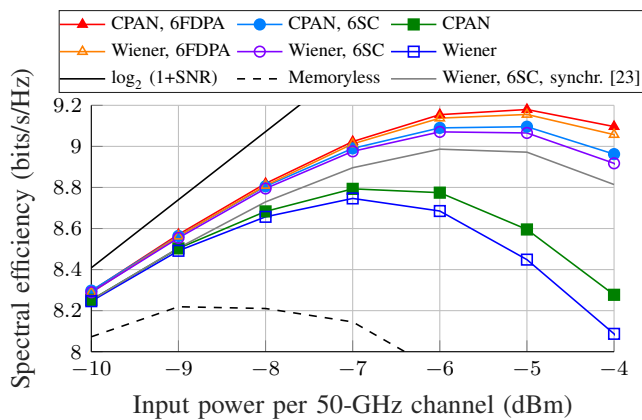


Fig. 5. Spectral efficiency for a 1-pol 1000-km link with the parameters in Table I and the frequency-dependent delays given by (100) and (102). The curve “Wiener, 6SC, synchr.” has all delays equal to 0 and uses the same scheme as the best curve from [23, Fig. 4(a)].

### B. Single Polarization System

Frequency-dependent delays increase rates for the 1-pol case too. Fig. 5 is the result of the simulations in [22] with the single-carrier delays (100) and the 6-subcarrier (6SC) delays

$$\Delta T_{6SC} = ((-37, -20, 4, 41, 41, -31), (42, 41, -2, 27, -33, -8), (37, 26, 41, 14, -42, 31), (39, 16, 23, 21, -10, 13), (-30, 18, -43, -21, -41, -37)) \frac{T_{6SC}}{90} \quad (102)$$

where  $T_{6SC} = 6T$ . These delays were chosen randomly. The gain of our system (CPAN model, 6 SC, FDPA, and the delays in (100) and (102)) over the best curve from [23] (Wiener model, 6SC, no delays) is 0.19 bits/s/Hz in spectral efficiency or 1.15 dB in power efficiency.

## IX. CONCLUSIONS

We extended the RP analysis of [15] to two polarizations and derived a 2pCPAN model for WDM transmission and the Manakov equation. The model includes phase noise, polarization rotation, and additive noise. We applied particle filtering to derive lower bounds on the capacity of the 2-pol optical channel. With multiple carriers, FDPA, and frequency-dependent delays, we improved existing bounds by 0.17 bits/s/Hz/pol in spectral efficiency or 0.8 dB in power efficiency.

Further improvements might be possible by modeling (73) as ISI, or by exploiting correlations of the phase noise and polarization rotation across subcarriers. Other ideas for future work are extensions to multi-mode communication and developing receivers that can achieve the reported gains.

## REFERENCES

- [1] C. Herard and A. Lacourt, “New multiplexing technique using polarization of light,” *Appl. Opt.*, vol. 30, no. 2, pp. 222–231, Jan 1991.
- [2] C. R. S. Fludger, T. Duthel, D. van den Borne, C. Schullien, E. Schmidt, T. Wuth, J. Geyer, E. De Man, G. Khoe, and H. de Waardt, “Coherent equalization and POLMUX-RZ-DQPSK for robust 100-GE transmission,” *J. Lightw. Technol.*, vol. 26, no. 1, pp. 64–72, 2008.
- [3] G. P. Agrawal, *Nonlinear Fiber Optics*, 4th ed. Academic Press, 2012.

- [4] M. Secondini, E. Agrell, E. Forestieri, D. Marsella, and M. R. Camara, “Nonlinearity mitigation in WDM systems: Models, strategies, and achievable rates,” *J. Lightw. Technol.*, vol. 37, no. 10, pp. 2270–2283, May 2019.
- [5] G. Kramer, M. I. Yousefi, and F. R. Kschischang, “Upper bound on the capacity of a cascade of nonlinear and noisy channels,” in *IEEE Inf. Theory Workshop*, April 2015, pp. 1–4.
- [6] M. I. Yousefi, G. Kramer, and F. R. Kschischang, “Upper bound on the capacity of the nonlinear Schrödinger channel,” in *IEEE Can. Workshop Inf. Theory*, July 2015, pp. 22–26.
- [7] H. Ghozlan and G. Kramer, “Models and information rates for multiuser optical fiber channels with nonlinearity and dispersion,” *IEEE Trans. Inf. Theory*, vol. 63, no. 10, pp. 6440–6456, 2017.
- [8] R. J. Essiambre, G. Kramer, P. J. Winzer, G. J. Foschini, and B. Goebel, “Capacity limits of optical fiber networks,” *J. Lightw. Technol.*, vol. 28, no. 4, pp. 662–701, Feb 2010.
- [9] P. Poggiolini, G. Bosco, A. Carena, V. Curri, Y. Jiang, and F. Forghieri, “The GN-model of fiber non-linear propagation and its applications,” *J. Lightw. Technol.*, vol. 32, no. 4, pp. 694–721, Feb 2014.
- [10] A. Carena, G. Bosco, V. Curri, Y. Jiang, P. Poggiolini, and F. Forghieri, “EGN model of non-linear fiber propagation,” *Opt. Express*, vol. 22, no. 13, pp. 16 335–16 362, Jun 2014.
- [11] A. Mecozzi, C. B. Clausen, and M. Shtaif, “Analysis of intrachannel nonlinear effects in highly dispersed optical pulse transmission,” *IEEE Photon. Technol. Lett.*, vol. 12, no. 4, pp. 392–394, 2000.
- [12] —, “System impact of intra-channel nonlinear effects in highly dispersed optical pulse transmission,” *IEEE Photon. Technol. Lett.*, vol. 12, no. 12, pp. 1633–1635, 2000.
- [13] A. Mecozzi, C. B. Clausen, M. Shtaif, Sang-Gyu Park, and A. H. Gnauck, “Cancellation of timing and amplitude jitter in symmetric links using highly dispersed pulses,” *IEEE Photon. Technol. Lett.*, vol. 13, no. 5, pp. 445–447, 2001.
- [14] A. Vannucci, P. Serena, and A. Bononi, “The RP method: a new tool for the iterative solution of the nonlinear Schrödinger equation,” *J. Lightw. Technol.*, vol. 20, no. 7, pp. 1102–1112, 2002.
- [15] A. Mecozzi and R. Essiambre, “Nonlinear Shannon limit in pseudolinear coherent systems,” *J. Lightw. Technol.*, vol. 30, no. 12, pp. 2011–2024, June 2012.
- [16] R. Dar, M. Feder, A. Mecozzi, and M. Shtaif, “Properties of nonlinear noise in long, dispersion-uncompensated fiber links,” *Opt. Express*, vol. 21, no. 22, pp. 25 685–25 699, Nov 2013.
- [17] R. Dar, M. Shtaif, and M. Feder, “New bounds on the capacity of the nonlinear fiber-optic channel,” *Opt. Lett.*, vol. 39, no. 2, pp. 398–401, Jan 2014.
- [18] Z. Tao, L. Dou, W. Yan, L. Li, T. Hoshida, and J. C. Rasmussen, “Multiplier-free intrachannel nonlinearity compensating algorithm operating at symbol rate,” *J. Lightw. Technol.*, vol. 29, no. 17, pp. 2570–2576, 2011.
- [19] P. Johannisson and M. Karlsson, “Perturbation analysis of nonlinear propagation in a strongly dispersive optical communication system,” *J. Lightw. Technol.*, vol. 31, no. 8, pp. 1273–1282, 2013.
- [20] M. Secondini and E. Forestieri, “Analytical fiber-optic channel model in the presence of cross-phase modulation,” *IEEE Photon. Technol. Lett.*, vol. 24, no. 22, pp. 2016–2019, Nov 2012.
- [21] M. Secondini, E. Forestieri, and G. Prati, “Achievable information rate in nonlinear WDM fiber-optic systems with arbitrary modulation formats and dispersion maps,” *J. Lightw. Technol.*, vol. 31, no. 23, pp. 3839–3852, Dec 2013.
- [22] F. J. García-Gómez and G. Kramer, “Mismatched models to lower bound the capacity of optical fiber channels,” *J. Lightw. Technol.*, vol. 38, no. 24, pp. 6779–6787, 2020.
- [23] M. Secondini, E. Agrell, E. Forestieri, and D. Marsella, “Fiber nonlinearity mitigation in WDM systems: Strategies and achievable rates,” in *Eur. Conf. Optical Commun.*, Sep. 2017, pp. 1–3.
- [24] S. Manakov, “On the theory of two-dimensional stationary self-focusing of electromagnetic waves,” *J. Experiment. Theoret. Physics*, vol. 65, pp. 505–516, 8 1973.
- [25] P. K. A. Wai and C. R. Menyuk, “Polarization mode dispersion, decorrelation, and diffusion in optical fibers with randomly varying birefringence,” *J. Lightw. Technol.*, vol. 14, no. 2, pp. 148–157, 1996.
- [26] R. Dar, M. Feder, A. Mecozzi, and M. Shtaif, “Pulse collision picture of inter-channel nonlinear interference in fiber-optic communications,” *J. Lightw. Technol.*, vol. 34, no. 2, pp. 593–607, 2016.
- [27] C. Czegledi, M. Karlsson, E. Agrell, and P. Johannisson, “Polarization drift channel model for coherent fibre-optic systems,” *Sci. Reports*, vol. 6, no. 21217, 2016.